ADVANCES IN ATMOSPHERIC SCIENCES, VOL. 31, SEPTEMBER 2014, 1167–1180

The Boreal Summer Intraseasonal Oscillation Simulated by Four Chinese AGCMs Participating in the CMIP5 Project

ZHAO Chongbo*[1], ZHOU Tianjun[2], SONG Lianchun[3], and REN Hongli[1]

[1]*Laboratory for Climate Studies, National Climate Center, China Meteorological Administration, Beijing* 100081

[2]*State Key Laboratory of Numerical Modeling for Atmospheric Sciences and Geophysical Fluid Dynamics, Institute of Atmospheric Physics, Chinese Academy of Sciences, Beijing* 100029

[3]*National Climate Center, China Meteorological Administration, Beijing* 100081

(Received 25 October 2013; revised 30 December 2013; accepted 10 February 2014)

ABSTRACT

The performances of four Chinese AGCMs participating in the Coupled Model Intercomparison Project Phase 5 (CMIP5) in the simulation of the boreal summer intraseasonal oscillation (BSISO) are assessed. The authors focus on the major characteristics of BSISO: the intensity, significant period, and propagation. The results show that the four AGCMs can reproduce boreal summer intraseasonal signals of precipitation; however their limitations are also evident. Compared with the Climate Prediction Center Merged Analysis of Precipitation (CMAP) data, the models underestimate the strength of the intraseasonal oscillation (ISO) over the eastern equatorial Indian Ocean (IO) during the boreal summer (May to October), but overestimate the intraseasonal variability over the western Pacific (WP). In the model results, the westward propagation dominates, whereas the eastward propagation dominates in the CMAP data. The northward propagation in these models is tilted southwest–northeast, which is also different from the CMAP result. Thus, there is not a northeast–southwest tilted rain belt revolution off the equator during the BSISO's eastward journey in the models. The biases of the BSISO are consistent with the summer mean state, especially the vertical shear. Analysis also shows that there is a positive feedback between the intraseasonal precipitation and the summer mean precipitation. The positive feedback processes may amplify the models' biases in the BSISO simulation.

Key words: boreal summer intraseasonal oscillation, AGCM, simulation, feedback

Citation: Zhao, C. B., T. J. Zhou, L. C. Song, and H. L. Ren, 2014: The boreal summer intraseasonal oscillation simulated by four Chinese AGCMs participating in the CMIP5 project. *Adv. Atmos. Sci.*, **31**(5), 1167–1180, doi: 10.1007/s00376-014-3211-7.

1. Introduction

The intraseasonal oscillation (ISO) is one of the most prominent large-scale sources of variability in the tropics and it undergoes a peculiar seasonal variation (Seo et al., 2005). While the strongly eastward propagating ISO (the Madden–Julian oscillation) is primarily observed in the boreal winter, the ISO in the boreal summer from May to October is dominated by the northward propagation over the Indian and western Pacific (Jiang et al., 2004). This boreal summer subseasonal mode significantly affects the active and break phases of the summer monsoon (Yasunari, 1979, 1980; Li et al., 2001). The wet and dry spells of the boreal summer intraseasonal oscillation (BSISO) strongly influence the extreme hydro-meteorological events, which cause about 80% of natural disasters (Lau and Waliser, 2005). The intraseasonal oscillation also has an effect on the formation, intensity, and course of the tropical cyclones (Nakazawa, 1986; Liebmann et al., 1994). Therefore, the BSISO is important for weather forecasting and climate prediction.

Numerical weather prediction results have shown that a model capable of simulating ISO may have a better overall forecasting ability (Li et al., 2006). However, attempts to simulate the BSISO have met with poor results (Slingo et al., 1996; Waliser et al., 2003; Lin et al., 2008; Sperber et al., 2013). This is because the BSISO shows a complex propagation process due to a prominent northeastward propagation associated with the monsoon over the Indian Ocean (IO) and the western Pacific (WP), as well as the formation of the summertime intertropical convergence zone off the equator (Sikka and Gadgil, 1980; Lau and Chan, 1986; Wang and Rui, 1990; Annamalai and Sperber, 2005; Seo et al., 2007). How to reliably simulate the BSISO has been a challenge to the climate-modeling community.

Over the Asian summer monsoon region, precipitation is an important forecast variable in model simulation. The outgoing longwave radiation (OLR) and the real-time multi-

* Corresponding author: ZHAO Chongbo
Email: chongbozhao@mail.iap.ac.cn

variate MJO (Madden–Julian oscillation) index (Wheeler and Hendon, 2004) focus on the deep convection and large-scale circumnavigate mode. During the boreal summer, the variability of the ISO is weaker than the MJO in the winter and propagates as far north as the Asian continent. The evaluation of precipitation is helpful in comprehensively examining the convective parameterization and topography description of the AGCMs. Lin et al. (2008) evaluated the intraseasonal precipitation during the boreal summer in the models participating in the IPCC Fourth Assessment Report (AR4). The results showed that the GCMs still have difficulties and display a wide range of ability in simulating the subseasonal variability. Our analysis is based on the atmospheric component of the four Chinese AGCM simulations, which were submitted to the ongoing Coupled Model Inter-comparison Project—Phase 5 (CMIP5). Specifically, the models we use are forced by the same observed SST, sea ice fractions, CO_2 concentrations, and other external forcing as defined in the Atmospheric Model Inter-comparison Project (AMIP) framework (Taylor et al., 2009). The aim of the study is to assess the performances of four new generation Chinese AGCMs in the simulation of BSISO and to understand the strengths and weaknesses of the models.

The remainder of the paper is organized as follows. The models and validation datasets used in this study are described in section 2. The results of the BSISO simulation are presented in section 3. A discussion of the model bias analysis and the relationship between the simulated mean state and BSISO are given in section 4. A summary is given in section 5.

2. Data, model, and analysis method

2.1. *Data*

To check the reliability of the model simulations, the pentad precipitation datasets are obtained from the Climate Prediction Center (CPC) Merged Analysis of Precipitation (CMAP) (Xie and Arkin, 1997) and the Global Precipitation Climatology Project (GPCP) Precipitation (Xie et al., 2003). The 3D zonal wind, meridional wind, and specific humidity datasets are used for analysis. These are obtained from the Climate Forecast System Reanalysis (CFSR; Saha et al., 2006; Saha et al., 2010) of the National Centers for Environmental Prediction (NCEP). Prior to the analysis, the pentad data are interpolated to daily values. We use nineteen (1979–97) summers (May to October) data for validating the simulations and discussing the biases.

2.2. *Models*

This analysis is based on 19 years of AMIP simulations from four Chinese AGCMs. In the AMIP run, the observed SST and sea ice temperature served as the boundary forcing of the numerical experiments. In addition, other conditions (CO_2 concentrations, solar constant, and aerosols) are also included during the integration.

Table 1 shows the acronyms, names, atmospheric models, resolutions, and convection parameterization schemes.

The BCC-CSM (Climate System Models developed by Beijing Climate Center) is a coupled climate system model including atmosphere, ocean, land surface, and sea ice components. There are two versions of this model with different horizontal resolutions, BCC-CSM1-1 and BCC-CSM1-1-m, that are participating in the CMIP5 (Jiang et al., 2012). In this paper, we focus on the former one. For the atmosphere, it uses an atmospheric general circulation model, BCC-AGCM2.1, developed by the Beijing Climate Center (BCC; Wu et al., 2008, 2010). This is a spectral model with horizontal T42 truncation ($\sim 2.8125^\circ$ horizontal resolution) and 26 layers in the vertical direction.

The BNU-ESM (Beijing Normal University-Earth System Model) is developed at the College of Global Change and Earth System Science at Beijing Normal University (Wu et al., 2013; http://esg.bnu.edu.cn/BNU_ESM_webs/htmls/index.html). For the atmosphere, BNU AGCM's horizontal resolution is T42 and the vertical resolution is 26 layers.

FGOALS-g2 (Flexible Global Ocean-Atmosphere-Land System Model, Grid-point Version 2) is developed at the State Key Laboratory of Numerical Modeling for Atmospheric Sciences and Geophysical Fluid Dynamics (LASG) at the Institute of Atmospheric Physics (IAP), Chinese Academy of Sciences (hereafter LASG/IAP) and Tsinghua University. The atmospheric component of FGOALS-g2 is the Grid Atmospheric Model of IAP/LASG (GAMIL), which employs a horizontal resolution of 2.8° between 65.58°N and 65.58°S

Table 1. List of models.

Modeling center	Abbreviation	Atmospheric model	Resolution	Convection parameterization scheme
Beijing Climate Center	BCC-CSM1-1	BCC_AGCM 2.1	T42, L26	Wu Scheme (Wu et al., 2010)
College of Global Change and Earth System Science, Beijing Normal University	BNU-ESM	BNU_AGCM	T42, L26	Standard Zhang–McFarlane with Convective Momentum Transports (Richter and Rasch, 2008)
LASG, Institute of Atmospheric Physics, Chinese Academy of Sciences and CESS, Tsinghua University	FGOALS-g2	GAMIL 2.0	$\sim 2.8^\circ \times 2.8^\circ$, L26	New Zhang–Mcfarlane (Zhang and Mu, 2002)
LASG, Institute of Atmospheric Physics, Chinese Academy of Sciences	FGOALS-s2	SAMIL 2.0	R42, L26	Tiedtke (1989)

and has 26 vertical layers. The details of the model are found in Li et al. (2013).

FGOALS-s2 (Flexible Global Ocean-Atmosphere-Land System Model, Spectral Version 2) is also developed at LASG/IAP. The atmospheric component of FGOALS-s2 is version 2.4.7 of Spectral Atmospheric Model in IAP/LASG (SAMIL; Bao et al., 2010, 2013), a spectral transform model with 26 atmospheric layers extending from the surface to 2.19 hPa, and with a horizontal resolution of R42 [$\sim 2.81^\circ$ (lon) $\times 1.66^\circ$ (lat)].

These models have updated their physical schemes to incorporate state-of-the-art research results. For example, the parameterizations for the deep cumulus convection, dry adiabatic adjustment, latent heat and sensible heat fluxes over the ocean surface, and the snow cover fraction were replaced with new schemes in BCC_AGCM2.0.1 Wu et al. (2010). In GAMIL2.0, the convection parameterization scheme was replaced by the Zhang–McFarlane scheme (Zhang and Mu, 2005), and a two-moment bulk stratiform cloud microphysics scheme (Morrison and Gettelman, 2008) was added to the microphysical processes (Li et al., 2013). Therefore, it is of interest to assess the simulations of BSISO in this new generation of climate models to look at the effects of the updated physical processes.

2.3. *Analysis method*

First, we estimate the reproduction quality of the BSISO's intensity, period, and propagation in turn. To extract the BSISO signal, daily precipitation, evaporation, specific humidity, and wind during 1979–97 are subject to a 20–100-day bandpass filtering based on harmonic decomposition (Kemball-Cook and Wang, 2001; Teng and Wang, 2003; Jiang et al., 2004). The 20–100-day bandpass filtered data from May to October in each year are then used as the intraseasonal component in the following analyses.

Next, to investigate the positive feedback between BSISO and the summer mean state, the moisture budget analysis are calculated according to Ray and Li (2013). To examine

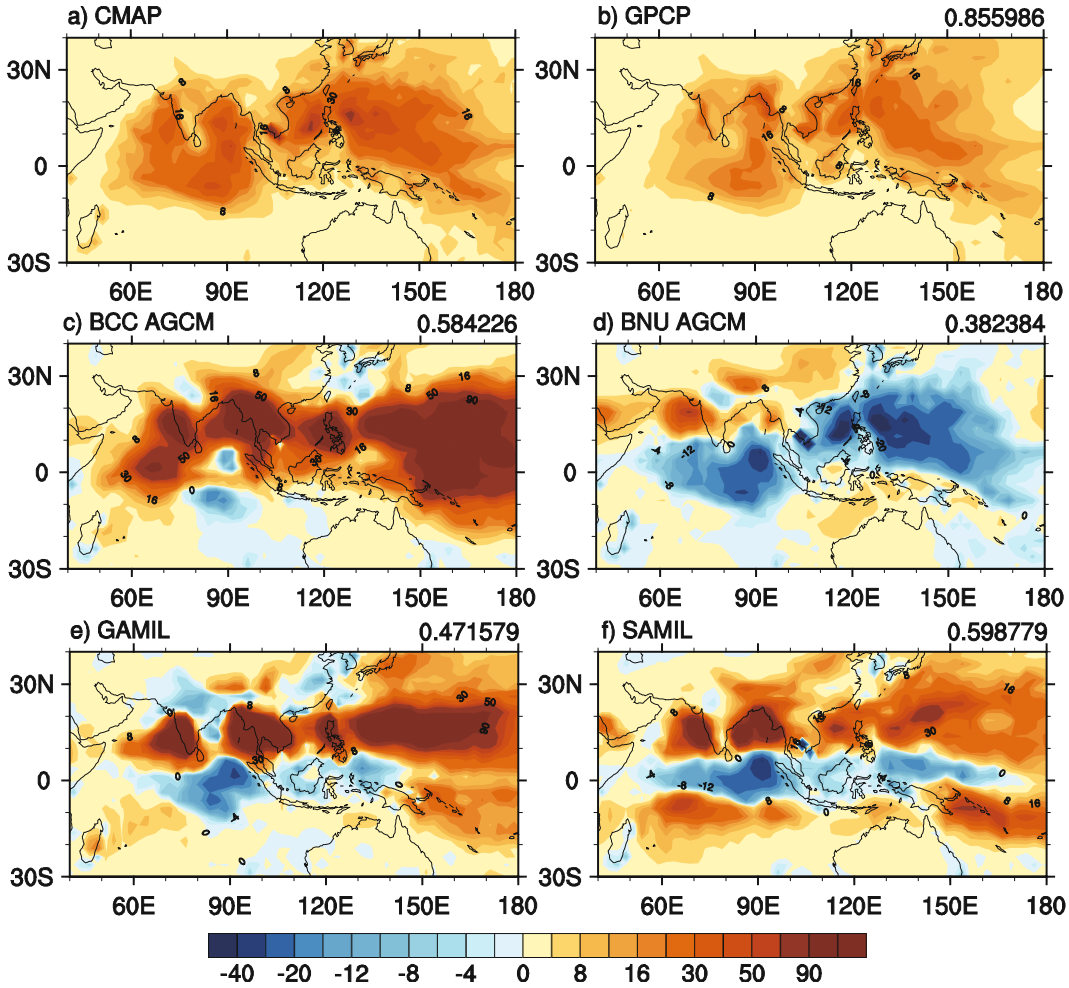

Fig. 1. Horizontal distribution of 20–100 day filtered precipitation variance of (a) CMAP, (b) GPCP and (c–f) the difference between models and CMAP (units: $mm^2\ d^{-2}$) during the boreal summer. The pattern correlations between models and CMAP are given at the top-right corner of each panel.

changes in precipitation, the summer mean vertically integrated moisture budget equation can be written as

$$\overline{\mathrm{Pr}} = \overline{E} + \overline{\langle -\boldsymbol{V}\cdot\nabla q\rangle} + \overline{\langle -q\nabla\cdot\boldsymbol{V}\rangle} + \overline{R}\,, \tag{1}$$

where Pr is precipitation, E is evaporation, $\boldsymbol{V}$ is horizontal velocity, q is specific humidity, and R is the residual term. $\langle -\boldsymbol{V}\cdot\nabla q\rangle$ is the advection of moisture term, $\langle -q\nabla\cdot\boldsymbol{V}\rangle$ is the moisture convergence term. The overbar, "–", represents the summer mean and "$\langle\ \rangle$" means the vertical integration and indicates a mass integration through the troposphere:

$$\langle\ \rangle = \int_{P_s}^{P_t} \frac{dP}{g}\,, \tag{2}$$

here P_t is 100 hPa, P_s is 1000 hPa, and g is gravity.

The summer mean moisture advection term, $\overline{\langle -\boldsymbol{V}\cdot\nabla q\rangle}$, can be further separated into two terms (Adv1 and Adv2)

$$\overline{\langle -\boldsymbol{V}\cdot\nabla q\rangle} = \langle -\overline{\boldsymbol{V}}\cdot\nabla\overline{q}\rangle + \overline{\langle -\boldsymbol{V}'\cdot\nabla q'\rangle} = \mathrm{Adv1} + \mathrm{Adv2}\,, \tag{3}$$

and the summer mean convergence term, $\overline{\langle -q\nabla\cdot\boldsymbol{V}\rangle}$, also can

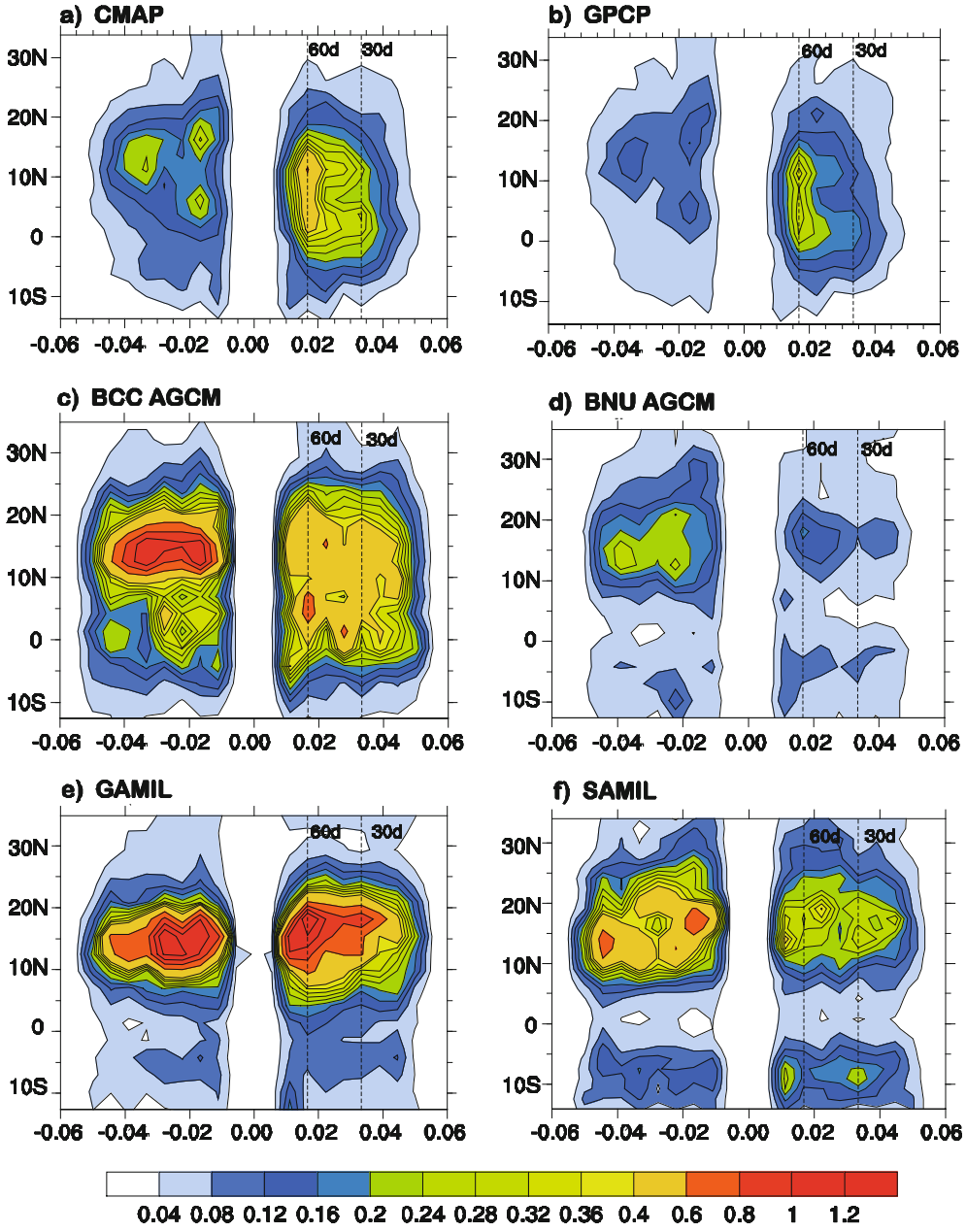

Fig. 2. Spectrum distribution of the eastward and westward propagating BSISO (units: $\mathrm{mm}^2\ \mathrm{d}^{-2}$) as a function of latitude and period for zonal wavenumber 1 (40°–180°E) from precipitation of CMAP, GPCP, BCC AGCM, BNU AGCM, GAMIL, and SAMIL.

be further separated into two terms (Con1 and Con2)

$$\overline{\langle -q\nabla\cdot\boldsymbol{V}\rangle} = \langle -\overline{q}\nabla\cdot\overline{\boldsymbol{V}}\rangle + \overline{\langle -q'\nabla\cdot\boldsymbol{V}'\rangle} = \mathrm{Con1} + \mathrm{Con2}\ , \quad (4)$$

here, the prime, "′", denotes the boreal summer intraseasonal perturbation, Adv1 represents the advection of the moisture by the summer mean wind, and Adv2 represents the summer mean advection of the intraseasonal moisture by the intraseasonal wind. Con1 denotes the convergence of summer mean moisture by the summer mean wind, and Con2 denotes the summer mean convergence of the intraseasonal moisture by the intraseasonal wind.

Through calculating the equations above during the boreal summer, the feedback correlation between the BSISO and the summer mean state can be derived.

3. Results of BSISO simulation

The reproduction quality of the BSISO's major characteristics is estimated first. Figure 1 shows the variance of the 20–100 day bandpass filtered precipitation anomaly during the boreal summer from 1979 to 1997. The most conspicuous

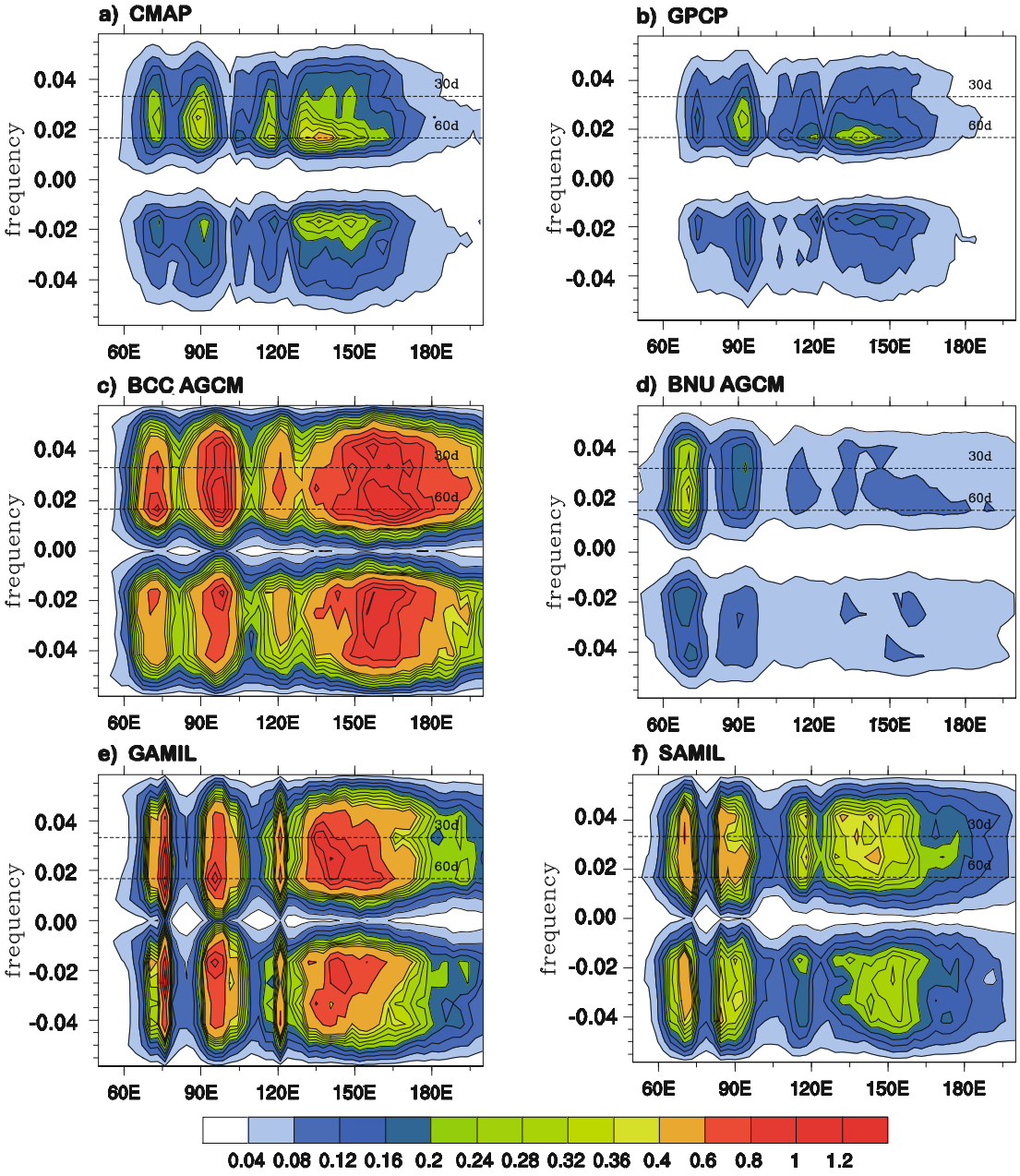

Fig. 3. Spectrum distribution of the northward and southward propagating BSISO (units: $\mathrm{mm}^2\ \mathrm{d}^{-2}$) as a function of longitude and period for meridional wavenumber 1 (15°S–25°N) from precipitation of CMAP, GPCP, BCC AGCM, BNU AGCM, GAMIL, and SAMIL.

feature of the precipitation intraseasonal variability in CMAP is two maxima: the tropical eastern IO and the WP. The horizontal distribution of the BSISO in the GPCP looks similar and has pattern correlations of 0.93 with the CMAP result. The models can replicate the BSISO signals; however there are still intensity biases in the two maxima areas. The four models all underestimate the variability over the tropical eastern IO. Three models (BCC AGCM, GAMIL, and SAMIL) overestimate the variability over the WP, but the BSISO is weaker in the BNU AGCM model than in the observation.

To provide a comprehensive evaluation of the period and propagation simulations on the BSISO, Figs. 2 and 3 show the zonal and meridional spectrum distribution at wavenumber 1 of the 20–100 days filtered precipitation anomaly. In the observation, separation of the eastward propagation and the westward propagation show that the eastward propagation of the BSISO is dominant and the strongest energy spectrum appears in the period of 30–90 days at zonal wavenumber 1 (corresponding to a wavelength from 40°E to 180°E) along the equator and 10°N. The highest westward propagation energy spectrum is concentrated at the 30–60 day period, and the location of the maxima is shifted northward compared with the eastward propagation. This indicates the northwestward propagation of the large-scale convection system in the WP, which is consistent with previous studies (Lau and Chan, 1986; Knutson and Weickmann, 1987). Models can reproduce the 30–90 day signals with the peak of 60 days, but the amplitude of the westward propagating mode of the BSISO is larger than the eastward counterpart.

In the observation, the northward propagation of the BSISO has its maxima over the IO and WP (Fig. 3). The significant period is around 40 days over the IO and 60 days over the WP, which means the BSISO propagates faster over the IO than over the WP. In the models' results, the northward propagation is well simulated, but the northward propagation is southwest–northeast tilted, which is also different from the

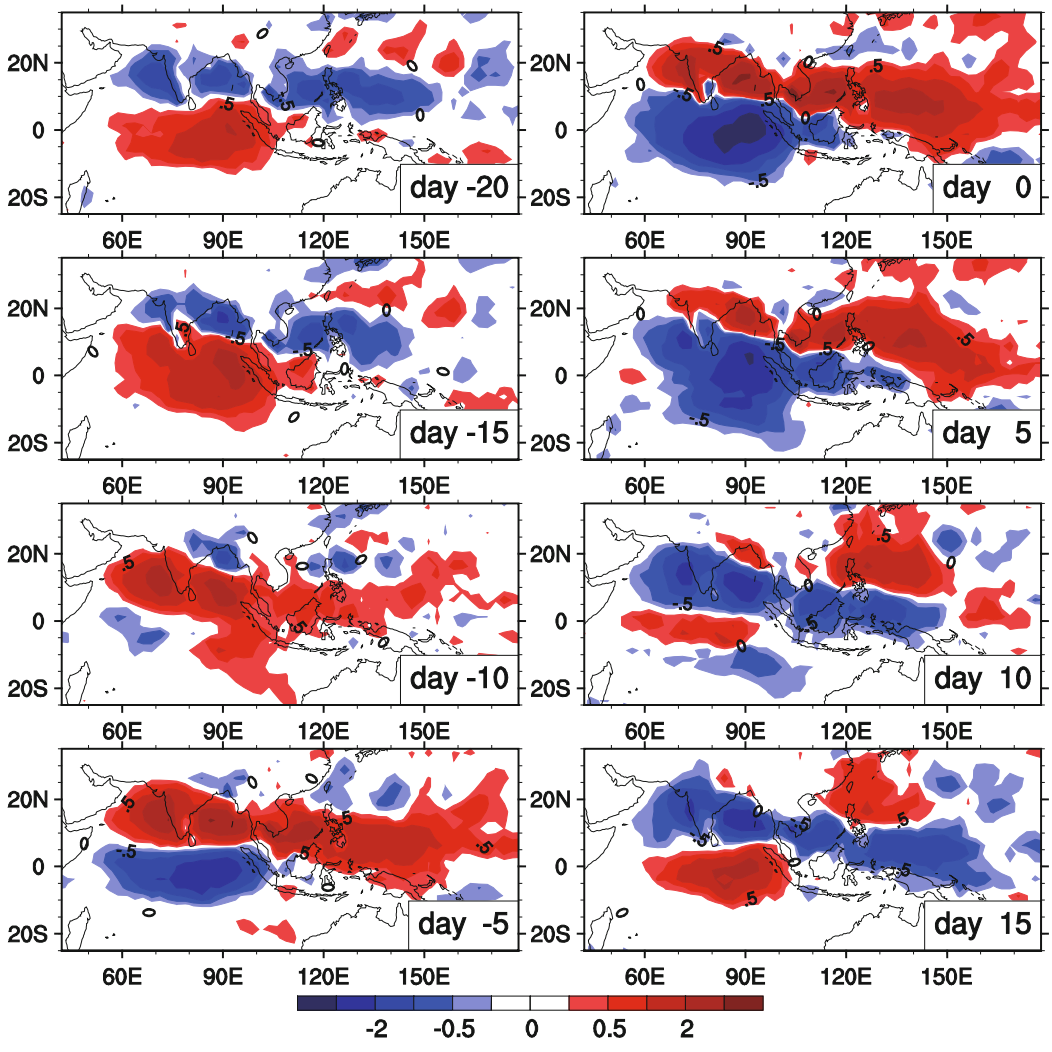

Fig. 4. Lag regression of 20–100 day bandpass filtered precipitation with PC-1 from day −20 to day 15 with 5-day intervals. The lag regressions have been scaled by one standard deviation of PC-1 to give units of mm d^{-1}.

CMAP result. This also can be seen in the lifecycle of the BSISO.

The time series of the first EOF mode that spans from 30°S to 30°N and 40°E to 180°E was used as the BSISO index (Jiang and Li, 2005; Zhao et al., 2013). Figure 4 shows the lag regressions of the 20–100 day filtered rainfall anomalies with PC-1. The regressions have been scaled by one standard deviation of PC-1. The pattern at day 0 resembles the first EOF mode pattern, as expected. During the observed BSISO lifecycle, rainfall is initiated over the southwestern IO around day −10, with a suppressed convective anomalies belt poleward over the IO and WP that propagates eastward. By day 10, the enhanced convection is mostly concentrated over the northern IO and tropical WP. At this time the suppressed BSISO phase dominates over the tropical Indian Ocean. The entire northwest–southeast tilted rainfall anomalies belt propagates northward (black line in Fig. 4).

Figure 5 shows the BSISO lifecycle patterns obtained from the BCC AGCM. The northward propagation of the rainfall anomalies band tilts southwest–northeast, though the essential evolution features seen in the lifecycle of CMAP are well represented. It is clear to see that the onset of positive rainfall anomalies occurs over the central Indian Ocean at day −10, and then propagates westward instead of eastward at day −5. The BSISO in the model result propagates more slowly over the IO than over the WP, which is opposite to the observation. This is also true with BNU AGCM, GAMIL, and SAMIL models (figure not shown). When the BSISO propagates northward faster over the WP than over the IO, positive rainfall anomalies first occur over the WP then the IO and the westward propagation is more significant than the eastward propagation.

These results demonstrate that the four Chinese models have the ability to capture the BSISO signals, but they are not perfect. The variance distribution shows a negative bias over the eastern IO. Over the WP, the variance in three of the models is larger than that in the observation, but is smaller in BNU AGCM. All the models show an overly strong west-

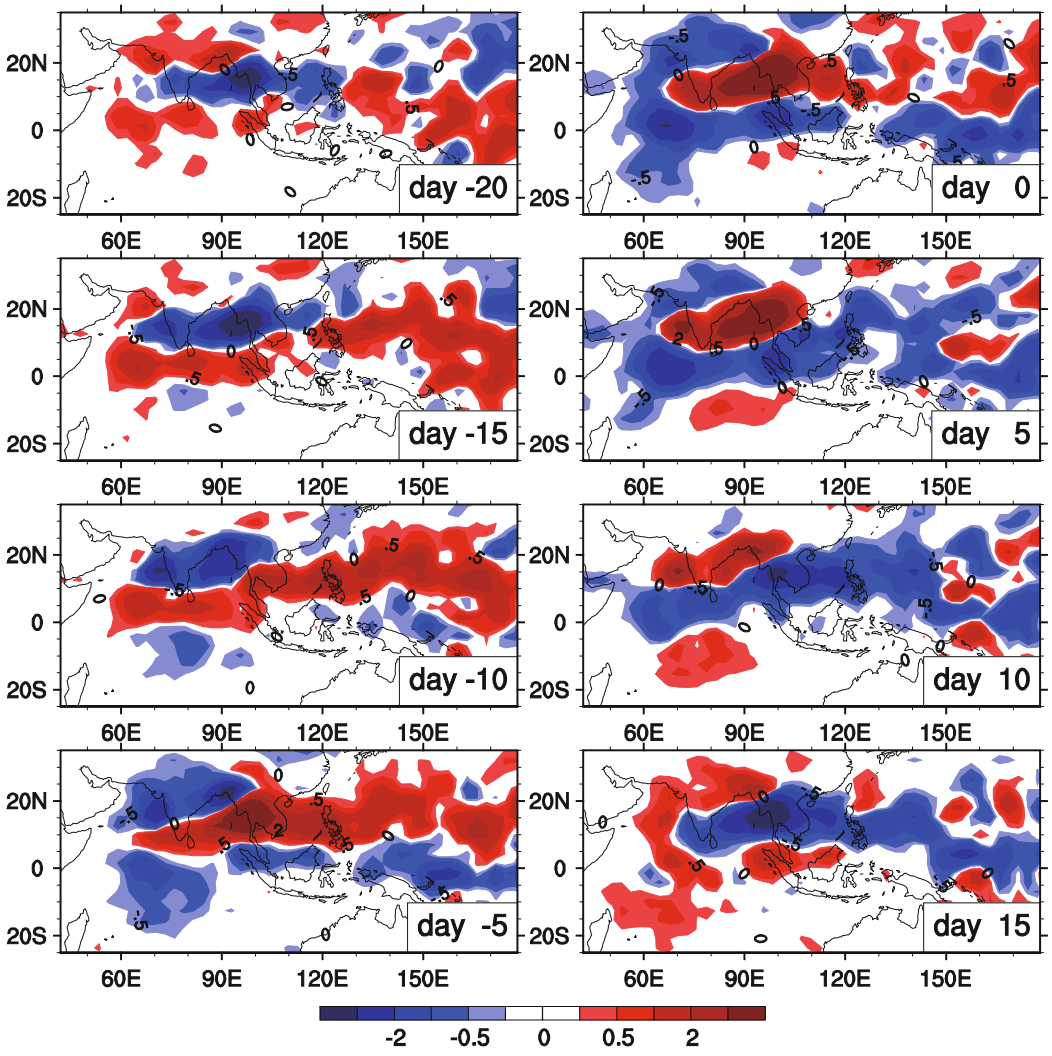

Fig. 5. The same as Fig. 4, except for BCC AGCM.

ward propagation and a southwest–northeast titled rainfall belt, which both have a relationship with the different northward propagation speed over the IO and WP. Next we present the possible cause of the models' bias.

4. Relationship between the simulated mean state and BSISO

4.1. *The effect of summer mean state on BSISO*

Previous observational studies indicate that the intensity of the ISO is highly correlated with the mean precipitation intensity (Wheeler and Kiladis, 1999; Ray and Li, 2013; Yang et al., 2013). The ability to reproduce the mean state is important for the models in simulating the ISO (Maloney and Hartman, 2001; Inness et al., 2003; Zhang et al., 2006). We assess the summer mean state in the model results and analyze the correlation between the BSISO and the summer mean state.

Figure 6 shows the summer mean precipitation. The observed summer precipitation (Figs. 6a and b) has two maxima: the tropical IO and WP. In the models, the summer mean precipitation is weaker over the tropical IO than it is in CMAP. BCC AGCM, GAMIL, and SAMIL overestimate the summer mean precipitation over the WP, whereas BNU AGCM underestimates it. This is consistent with the bias of the BSISO variance simulation. Since the greater precipitation along the Pacific Intertropical Convergence Zone may lead to a stronger Rossby wave response and a suppressed Kelvin wave, the westward propagation is excessive in the models.

There is a close relationship between the easterly shear and the precipitation intensity over the tropical IO and WP, since the strength of the zonal wind along the convective center's sides is synchronous with the tropical convection activity. The CFSR reanalysis result (Fig. 7a) has lower tro-

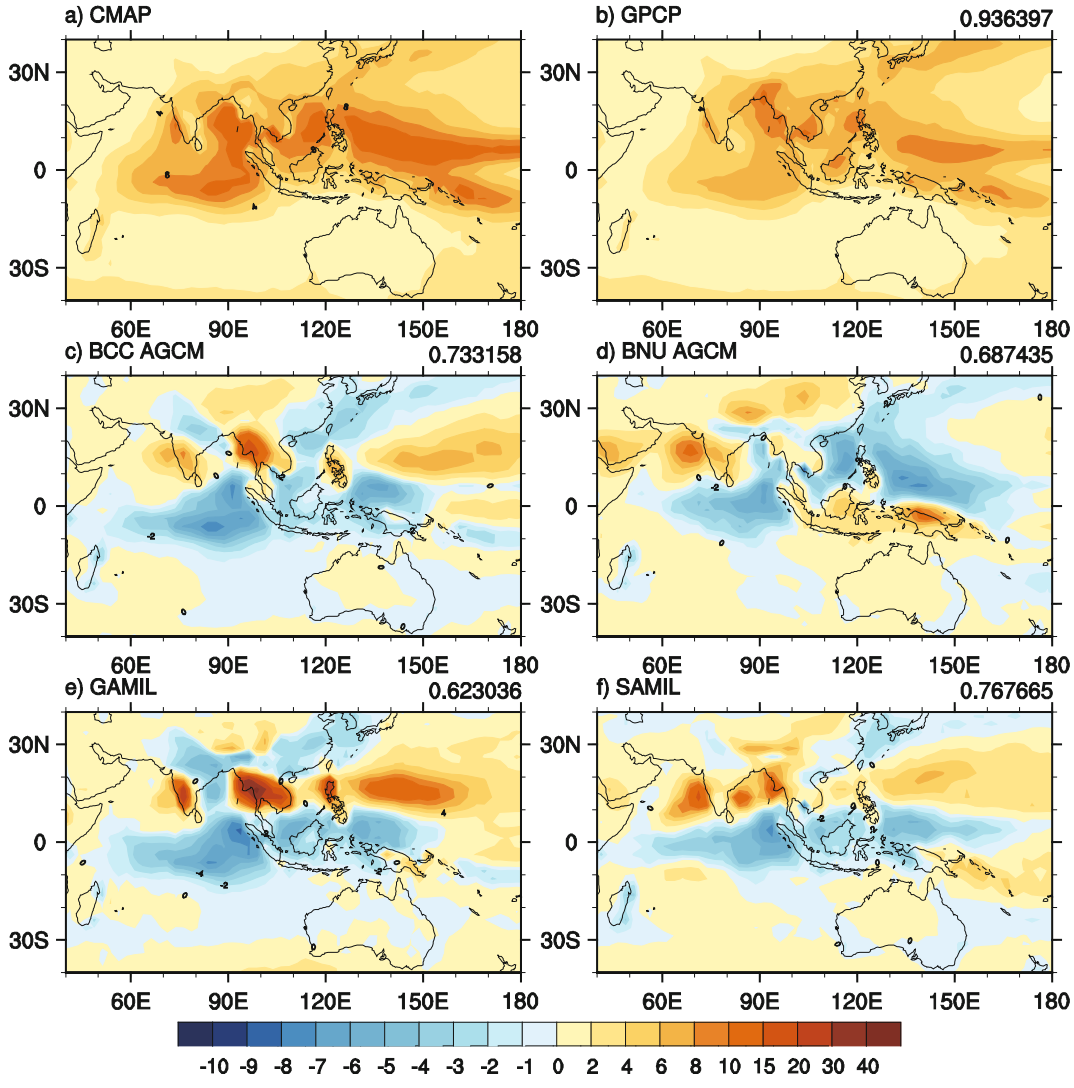

Fig. 6. Summer mean precipitation of (a) CMAP, (b) GPCP and (c–f) the difference between models and CMAP (units: mm d^{-1}). The pattern correlations between models and CMAP are given at the top-right corner of each panel.

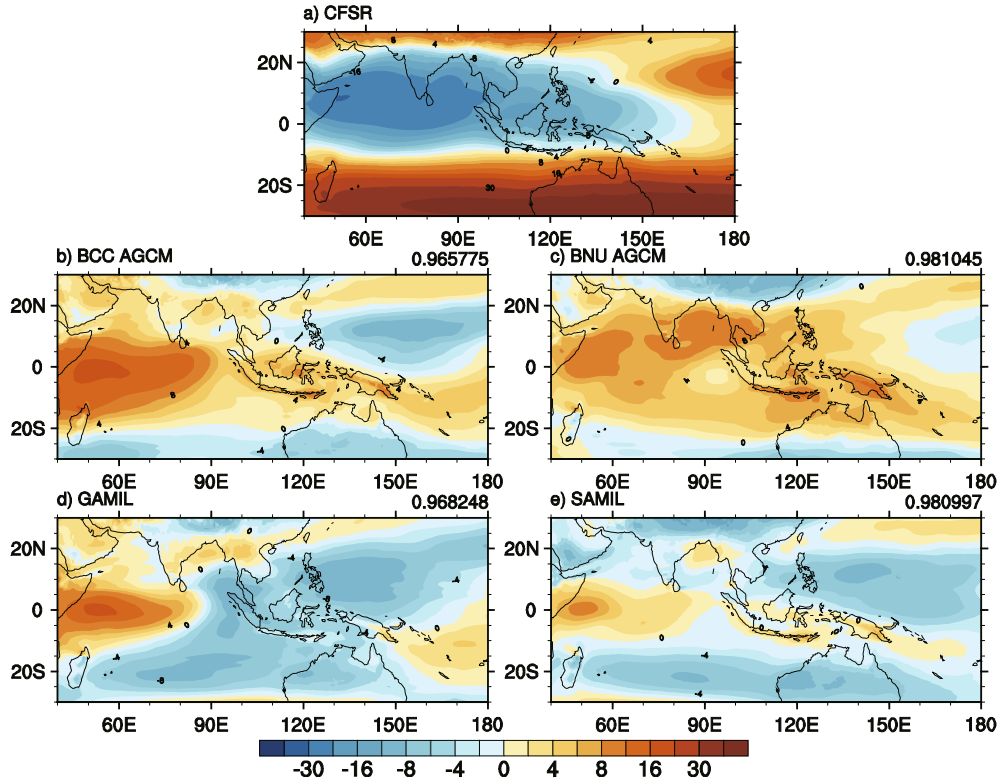

Fig. 7. Summer mean vertical shear ($U_{200} - U_{850}$) of (a) CFSR and (b–e) the difference between models and CFSR (units: m s^{-1}). The pattern correlations between models and CFSR are given at the top-right corner of each panel.

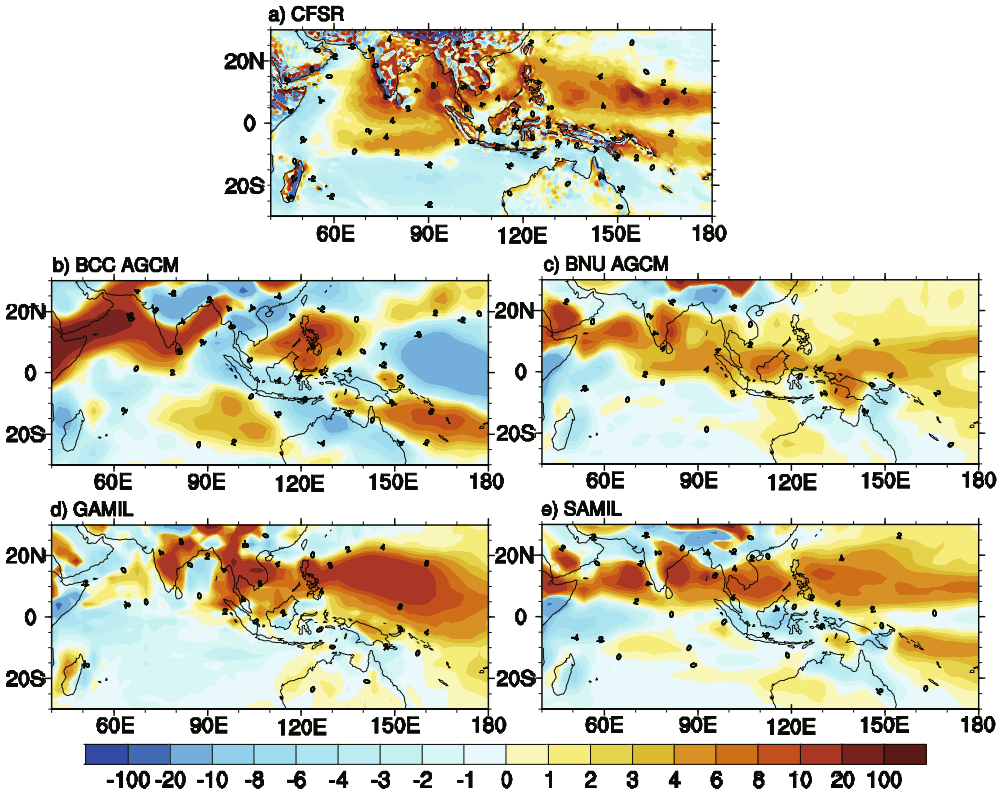

Fig. 8. Summer mean moisture convergence ($\overline{\langle -q\nabla \cdot \boldsymbol{V} \rangle}$) of CFSR, BCC AGCM, BNU AGCM, GAMIL, and SAMIL (units: mm d^{-1}).

pospheric westerlies and upper tropospheric easterlies over the IO and WP during the boreal summer. The models capture the observed summer mean wind well; however, both the westerlies in the lower troposphere and the easterlies in the upper troposphere are underestimated over the IO. Therefore, the summer mean vertical shear ($U_{200} - U_{850}$) is weak in the model results (Figs. 7b–d). Over the WP, the vertical shear is too strong in these models, apart from BNU AGCM. The summer mean easterly shear biases may exercise a great influence on the BSISO simulation. Wang and Xie (1997) found that the easterly vertical shear can remarkably enhance the Rossby wave emanation in the western North Pacific and their development in the monsoon region, playing an essential role in sustaining the ISO in the off-equatorial monsoon regions. Jiang et al. (2004) proposed that the key process associated with the BSISO is the generation of barotropic vorticity due to the coupling between the free-atmosphere baroclinic and barotropic modes in the presence of the vertical shear of the mean flow. The induced barotropic vorticity in the free atmosphere further causes a moisture convergence in the planetary boundary layer, leading to the northward shift of the convective heating.

With a reduced easterly shear over the IO in the four Chinese models, the tropical intraseasonal activity is reduced and the northward propagation is also suppressed. With an increased easterly shear over the WP in BCC AGCM, GAMIL, and SAMIL, the intraseasonal activity is increased and the northward propagation is favored.

4.2. *BSISO upscale feedback to summer mean state*

We further investigate the BSISO feedback to the summer mean state which is responsible for the BSISO simulation biases through the moisture budget analysis. Figure 8 shows the distribution of the boreal summer mean moisture convergence term ($\overline{\langle -q\nabla\cdot\boldsymbol{V}\rangle}$) in Eq. (1). In the CFSR result, the marked precipitation maxima are primarily attributed to this positive moisture convergence term (Fig. 8a), and it has a similar distribution to the summer mean precipitation. In the model results, the moisture convergence pattern (Figs. 8b–e) is also very similar to the distribution of the summer mean precipitation, suggesting that moisture convergence plays a key role in explaining the summer mean precipitation biases.

Figure 9 shows the contributions from the moisture convergence decomposition term Con2 [see Eq. (4)]. The calculation suggests that the convergence of the intraseasonal moisture by intraseasonal winds is conducive to the positive boreal summer mean moisture convergence in the region with

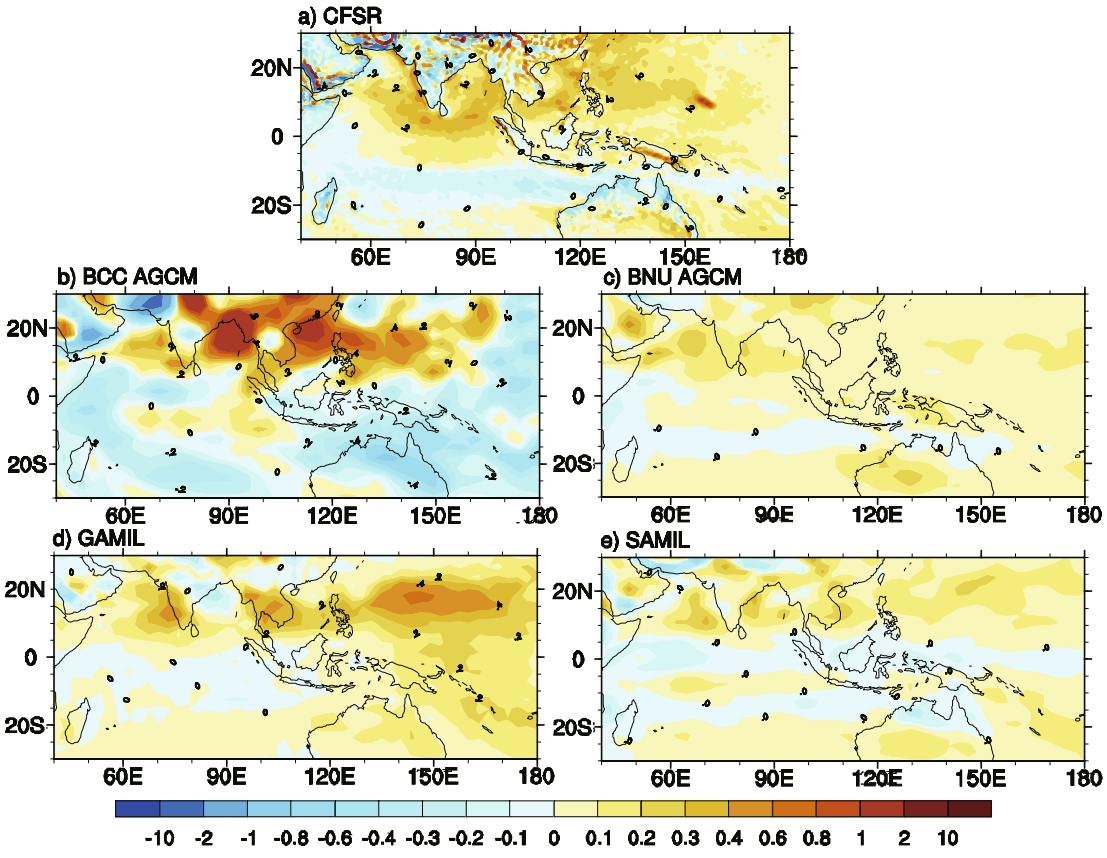

Fig. 9. Summer mean term Con2 ($\overline{\langle -q'\nabla\cdot\boldsymbol{V}'\rangle}$) of CFSR, BCC AGCM, BNU AGCM, GAMIL, and SAMIL (units: mm d^{-1}).

maxima precipitation (Fig. 9). The nonlinear interaction between the intraseasonal fields plays a positive role in the summer mean precipitation, and the Con2 term accounts for about 5% of the summer mean precipitation over the IO. This positive feedback of the BSISO on the summer mean state may further influence the BSISO simulation itself.

The in-phase relationship between the intraseasonal moisture and intraseasonal convergence can affect the summer mean precipitation (Ray and Li, 2013). The intraseasonal convergence and wet anomaly accompany the positive phase (enhanced convection) of ISO, and vice versa, the intraseasonal and dry anomalies accompany the negative phase (suppressed convection) of ISO (Hsu and Li, 2012). As a result, the summer mean Con2 is positive and conducive to promoting a positive contribution to the summer mean precipitation. The synchronous relationship is significant over the IO and WP where the summer mean precipitation and moisture convergence are overly underestimated or overestimated in the model results (Fig. 10).

5. Summary and concluding remarks

The performance of four Chinese AGCMs in reproducing the intraseasonal precipitation during boreal summer has been assessed.

Compared with the CMAP data, over the eastern tropical IO all the models produce insufficient BSISO amplitude, whereas over the WP, BCC-CSM1-1, GAMIL, and SAMIL give an excessive BSISO amplitude, and BNU AGCM gives an inadequate BSISO amplitude. Also, an overly westward propagation and a southwest–northeast tilted northward propagation are found in the model results.

By comparing the models with each other, both BCC AGCM and SAMIL have higher correlations with the observation in the BSISO variance pattern simulation. BNU AGCM and SAMIL both have a greater ratio between the eastward and westward propagations. BNU AGCM reproduces more reasonable periodicity over the IO and WP regions (Fig. 11).

The possible reason for the bias for both the summer mean tropical precipitation and the BSISO variance in the models is analyzed by calculating the vertical shear and diagnosing the time-averaged vertically integrated moisture budget equation. The major results are summarized below.

In the models, the background easterly vertical shear is weaker (stronger), accompanied by a weaker (stronger) summer mean precipitation than the observation. This decrease (increase) causes the decrease (increase) of intraseasonal activity and the suppression (enhancement) of the BSISO northward propagation. The induced weaker (stronger) BSISO humidity and wind further leads to less (more) contribution to the summer mean precipitation, through the nonlinear interaction of the intraseasonal moisture and intraseasonal convergence term. This positive feedback between the summer mean state and the BSISO may eventually lead to a significant deviation of the BSISO variance.

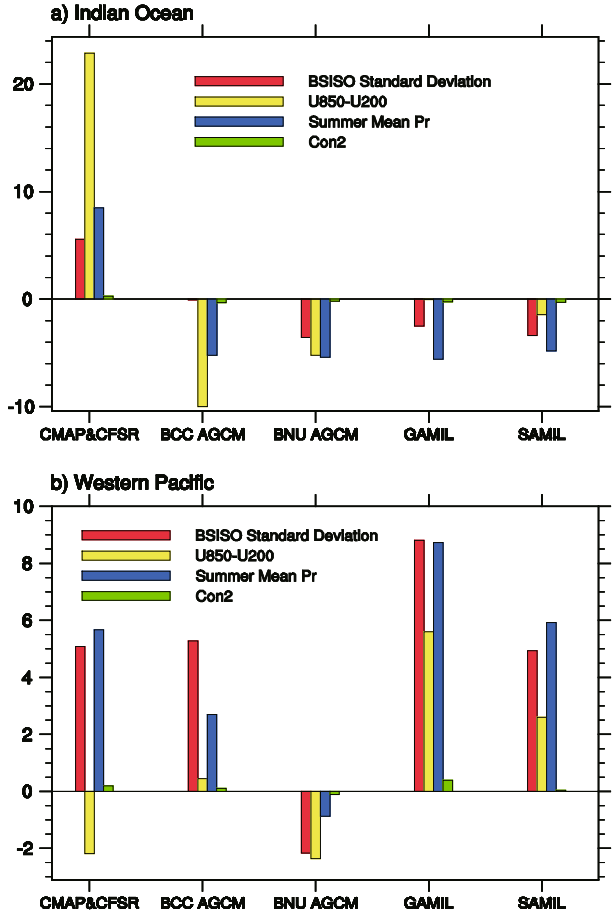

Fig. 10. The BSISO standard deviation (units: $mm^2\ d^{-2}$), vertical shear (units: $m\ s^{-1}$), summer mean precipitation (units: $mm\ d^{-1}$), and Con2 term (units: $mm\ d^{-1}$) of CMAP/CFSR and the difference between models and CMAP/CFSR over (a) IO (2°N, 87°E) and (b) WP (20°N, 145°E).

To improve the model simulation of the BSISO, the mean state calibration is not enough. The ratio between ISO variability and other subseasonal variability also needs to be adjusted. Compared with the observation, the BSISO in the models is not the dominant signal in the total subseasonal variation. Both of the observational datasets (CMAP and GPCP) have prominent spectral peaks between the 10- and 60-day periods over the IO, and the 10- and 75-day periods over the WP. In the models' results, compared to the BSISO signal, the higher and lower frequency signals are more significant in the total subseasonal perturbation (Fig. 11). The results reveal two common biases in the four models, i.e., a higher frequency and too strong persistence of equatorial precipitation. In the models, the higher and lower frequency signals are overpowered due to the easy initiation and overly strong persistence of equatorial precipitation. These biases may be ascribed to the convection parameterization process, model resolution, and vertical heating profile in atmospheric models, which are essential for the BSISO simulation (Lin et al., 2008; Jia et al., 2009; Li et al., 2009).

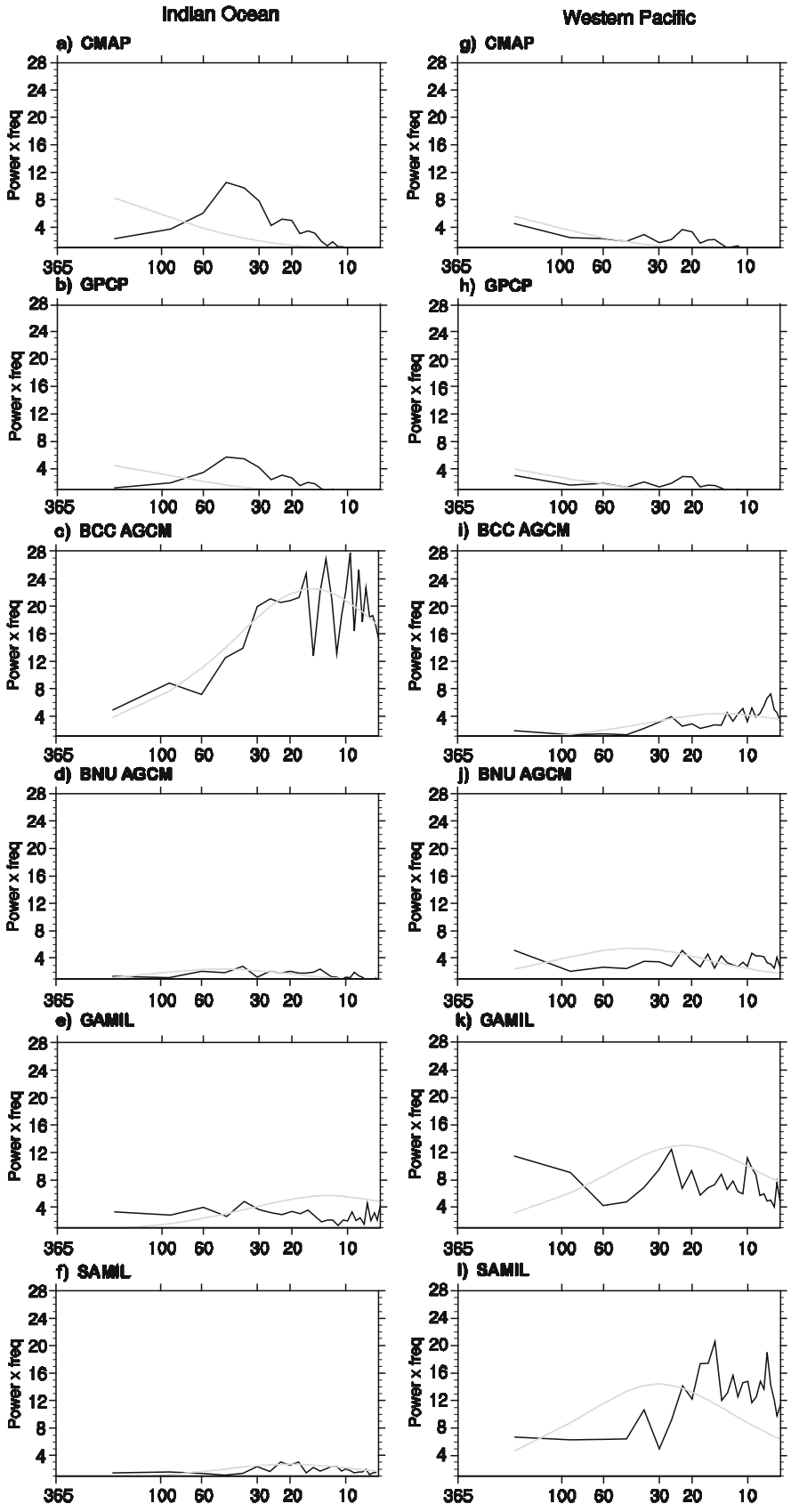

Fig. 11. Spectrum of precipitation over (a–f) IO (5°S–0°N, 50°–100°E) and (g–l) WP (10°–15°N, 110°–160°E) for CMAP, GPCP, BCC AGCM, BNU AGCM, GAMIL, and SAMIL (units: $mm^2\ d^{-2}$).

Acknowledgements. This study is jointly supported by the National Basic Research and Development (973) Program of China (Grant No. 2012CB955902), China Meteorological Special Project (Grant Nos. GYHY201206016 and GYHY 201406022), National Natural Science Foundation of China (Grant No. 41125017) and the Public science and technology research funds projects of ocean (Grant No. 201105019-3).

REFERENCES

Annamalai, H., and K. R. Sperber, 2005: Regional heat sources and the active and break phases of boreal summer intraseasonal (30–50 day) variability. *J. Atmos. Sci.*, **62**, 2726–2748.

Bao, Q., G. X. Wu, Y. M. Liu, J. Yang, Z. Z. Wang, and T. J. Zhou, 2010: An introduction to the coupled model FGOALS1.1-s and its performance in East Asia. *Adv. Atmos. Sci.*, **27**, 1131–1142, doi: 10.1007/s00376-010-9177-1.

Bao, Q., and Coauthors, 2013: The flexible global ocean-atmosphere-land system model, spectral version 2: FGOALS-s2. *Adv. Atmos. Sci.*, **30**, 561–576, doi: 10.1007/s00376-012-2113-9.

Hsu, P. C., and T. Li, 2012: Role of the boundary layer moisture asymmetry in causing the eastward propagation of the Madden-Julian Oscillation. *J. Climate*, **25**, 4914–4931.

Inness, P. M., J. M. Slingo, E. Guilyardi, and J. Cole, 2003: Simulation of the Madden-Julian oscillation in a coupled general circulation model. Part II: The role of the basic state. *J. Climate*, **16**, 365–382.

Jia, X. L., C. Y. Li, N. F. Zhou, and J. Ling, 2009: The MJO in an AGCM with three different cumulus parameterization schemes. *Dyn. Atmos. Oceans*, **49**, 141–163.

Jiang, J. H., and Coauthors, 2012: Evaluation of cloud and water vapor simulations in CMIP5 climate models using NASA "A-Train" satellite observations. *J. Geophys. Res.*, **117**, D14105, doi: 10.1029/2011JD017237.

Jiang, X., and T. Li, 2005: Reinitiation of the boreal summer intraseasonal oscillation in the tropical Indian Ocean. *J. Climate*, **18**, 3777–3795.

Jiang, X., T. Li, and B. Wang, 2004: Structures and mechanisms of the northward propagating boreal summer intraseasonal oscillation. *J. Climate*, **17**, 1022–1039.

Kemball-Cook, S., and B. Wang, 2001: Equatorial waves and air-sea interaction in the boreal summer intraseasonal oscillation. *J. Climate*, **14**, 2923–2942.

Knutson, T. R., and K. M. Weickmann, 1987: 30–60-day atmospheric oscillations: Composite life cycles of convection and circulation anomalies. *Mon. Wea. Rev.*, **115**, 1407–1436.

Lau, K. M., and P. H. Chan, 1986: Aspects of the 40–50 day oscillation during the northern summer as inferred from the outgoing longwave radiation. *Mon. Wea. Rev.*, **114**, 1354–1367.

Lau, W. K. M., and D. E. Waliser, Eds., 2005: *Intraseasonal Variability of the Atmosphere-Ocean Climate System*. Springer, Heidelberg, 614 pp.

Li, C. Y., Z. X. Long, and Q. Y. Zhang, 2001: Strong/weak summer monsoon activity over the South China Sea and atmospheric intraseasonal oscillation. *Adv. Atmos. Sci.*, **18**, 1146–1160.

Li, C. Y., X. L. Jia, J. A. Ling, W. Zhou, and C. D. Zhang, 2009: Sensitivity of MJO simulations to convective heating profiles. *Climate Dyn.*, **32**, 167–187.

Li, L. J., and Coauthors, 2013: The flexible global ocean-atmosphere-land system model, Grid-point Version 2: FGOALS-g2. *Adv. Atmos. Sci.*, **30**, 543–560, doi: 10.1007/s00376-012-2140-6.

Li, T., X. Jia, and M. Dong, 2006: The importance of the atmospheric intraseasonal oscillation in the prediction of the weather and climate. *Acta Meteorologica Sinica*, **64**, 412–419. (in Chinese)

Liebmann, B., H. H. Hendon, and J. D. Glick, 1994: The relationship between tropical cyclones of the western Pacific and Indian Oceans and the Madden-Julian oscillation. *J. Meteor. Soc. Japan*, **72**, 401–411.

Lin, J. L., K. M. Weickman, G. N. Kiladis, B. E. Mapes, S. D. Schubert, M. J. Suarez, J. T. Bacmeister, and M. I. Lee, 2008: Subseasonal variability associated with Asian summer monsoon simulated by 14 IPCC AR4 coupled GCMs. *J. Climate*, **21**, 4541–4567.

Maloney, E. D., and D. L. Hartman, 2001: The sensitivity of intraseasonal variability in the NCAR CCM3 to changes in convective parameterization. *J. Climate*, **14**, 2015–2034.

Morrison, H., and A. Gettelman, 2008: A new two-moment bulk stratiform cloud microphysics scheme in the community atmosphere model, version 3 (CAM3). Part I: Description and numerical tests. *J. Climate*, **21**, 3642–3659.

Nakazawa, T., 1986: Intraseasonal variations of OLR in the tropics during the FGGE year. *J. Meteor. Soc. Japan*, **64**, 17–34.

Ray, P., and T. Li, 2013: Relative roles of circumnavigating waves and extratropics on the MJO and its relationship with the mean state. *J. Atmos. Sci*., **70**, 876–893.

Saha, S., and Coauthors, 2006: The NCEP climate forecast system. *J. Climate*, **19**, 3483–3517.

Saha, S., and Coauthors, 2010: The NCEP climate forecast system reanalysis. *Bull. Amer. Meteor. Soc.*, **91**, 1015–1057.

Seo, K.-H., J.-K. Schemm, C. Jones, and S. Moorthi, 2005: Forecast skill of the Tropical Intraseasonal Oscillation in the NCEP GFS dynamical extended range forecasts. *Climate Dyn.*, **25**, 265–284.

Seo, K.-H., J.-K. E. Schemm, W. Wang, and A. Kumar, 2007: The boreal summer intraseasonal oscillation simulated in the NCEP Climate Forecast System (CFS): The effect of sea surface temperature. *Mon. Wea. Rev.*, **135**, 1807–1827.

Sikka, D. R., and S. Gadgil, 1980: On the maximum cloud zone and the ITCZ over Indian longitudes during the southwest monsoon. *Mon. Wea. Rev.*, **108**, 1840–1853.

Slingo, J. M., and Coauthors, 1996: Intraseasonal oscillation in 15 atmospheric general circulation models: Results from an AMIP diagnostic subproject. *Climate Dyn.*, **12**, 325–357.

Sperber, K. R., H. Annamalai, I.-S. Kang, A. Kitoh, A. Moise, A. Turner, B. Wang, and T. Zhou, 2013: The Asian summer monsoon: An intercomparison of CMIP5 vs. CMIP3 simulations of the late 20th century. *Climate Dyn.*, **41**, 2711–2744, doi: 10.1007/s00382-012-1607-6.

Taylor, K. E., R. J. Stouffer, and G. A. Meehl, 2009: A summary of the CMIP5 experiment design. [Available online at http://cmip-pcmdi.llnl.gov/cmip5/docs/Taylor-CMIP5-design.pdf]

Teng, H., and B. Wang, 2003: Interannual variations of the boreal summer intraseasonal oscillation in the Asian-Pacific region. *J. Climate*, **16**, 3572–3584.

Waliser, D. E., and Coauthors, 2003: AGCM simulations of intraseasonal variability associated with the Asian summer monsoon. *Climate Dyn.*, **21**, 423–446.

Wang, B., and H. Rui, 1990: Synoptic climatology of transient tropical intraseasonal convection anomalies. *Meteor. Atmos. Phys.*, **44**, 43–61.

Wang, B., and X. Xie, 1997: A Model for the Boreal Summer Intraseasonal Oscillation. *J. Atmos. Sci.*, **54**, 72–86.

Wheeler, M. C., and G. N. Kiladis, 1999: Convectively coupled equatorial waves: Analysis of clouds and temperature in the wavenumber-frequency domain. *J. Atmos. Sci.*, **56**, 374–399.

Wheeler, M. C., and H. Hendon, 2004: An All-Season Real-Time multivariate MJO index: Development of an index for monitoring and prediction. *Mon. Wea. Rev.*, **132**, 1917–1932.

Wu, Q. Z., J. M. Feng, W. J. Dong, L. N. Wang, D. Y. Ji, and H. Q. Cheng, 2013: Introduction of the CMIP5 experiments carried out by BNU-ESM. *Progressus Inquisitiones de Mutatione Climatis*, **9**, 291–294.

Wu, T. W., R. C. Yu, and F. Zhang, 2008: A modified dynamic framework for the atmospheric spectral model and its application. *J. Atmos. Sci.*, **65**, 2235–2253.

Wu, T. W., and Coauthors, 2010: The Beijing climate center for atmospheric general circulation model (BCC AGCM 2.0.1): Description and its performance for the present-day climate. *Climate Dyn.*, **34**, 123–147.

Xie, P., and P. A. Arkin, 1997: Global precipitation: A 17-year monthly analysis based on gauge observations, satellite estimates, and numerical model outputs. *Bull. Amer. Meteor. Soc.*, **78**, 2539–2558.

Xie, P., and Coauthors, 2003: GPCP pentad precipitation analyses: An experimental dataset based on gauge observations and satellite estimates. *J. Climate*, **16**, 2197–2214.

Yang, J., Q. Bao, and X. C. Wang, 2013: Intensified eastward and northward propagation of tropical intraseasonal oscillation over the equatorial Indian Ocean in a global warming scenario. *Adv. Atmos. Sci.*, **30**, 167–174, doi: 10.1007/s00376-012-1260-3.

Yasunari, T., 1979: Cloudiness fluctuations associated with the northern hemisphere summer monsoon. *J. Meteor. Soc. Japan*, **57**, 227–242.

Yasunari, T., 1980: A quasi-stationary appearance of 30 to 40 day period in the cloudiness fluctuations during the summer monsoon over India. *J. Meteor. Soc. Japan*, **58**, 225–229.

Zhang, C, M. Dong, S. Gualdi, H. H. Hendon, E. D. Maloney, A. Marshall, K. R. Sperber, and W. Wang, 2006: Simulations of the Madden-Julian oscillation by four pairs of coupled and uncoupled global models. *Climate Dyn.*, **27**, 573–592.

Zhang, G. J., and M. Mu, 2005: Effects of modifications to the Zhang-McFarlane convection parameterization on the simulation of the tropical precipitation in the national center for atmospheric research community climate model, version 3. *J. Geophys. Res.*, **110**, D09109, doi: 10.1029/2004JD005617.

Zhao, C. B., T. Li, and T. J. Zhou, 2013: Precursor signals and processes associated with MJO initiation over the Tropical Indian Ocean. *J. Climate*, **26**, 291–307.